Journal of Astronomical Telescopes, Instruments, and Systems

AstronomicalTelescopes.SPIEDigitalLibrary.org

Hydroxide catalysis bonding of Allvar Alloy 30, a negative thermal expansion alloy

Kaden J. Loring
Luis F. Ortega
James A. Monroe
Jeremy S. McAllister
Xavier Huerta
Guido Mueller
Paul Fulda

SPIE.

Kaden J. Loring, Luis F. Ortega, James A. Monroe, Jeremy S. McAllister, Xavier Huerta, Guido Mueller, Paul Fulda, "Hydroxide catalysis bonding of Allvar Alloy 30, a negative thermal expansion alloy," *J. Astron. Telesc. Instrum. Syst.* **6**(1), 015007 (2020), doi: 10.1117/1.JATIS.6.1.015007

Hydroxide catalysis bonding of Allvar Alloy 30, a negative thermal expansion alloy

Kaden J. Loring,[a,*] Luis F. Ortega,[a] James A. Monroe,[b] Jeremy S. McAllister,[b] Xavier Huerta,[c] Guido Mueller,[a] and Paul Fulda[a]

[a]University of Florida, Department of Physics, Gainesville, Florida, United States
[b]Allvar, College Station, Texas, United States
[c]Texas A&M University, Department of Mechanical Engineering, College Station, Texas, United States

Abstract. Many future space missions including Large UV/Optical/Infrared Surveyor and Laser Interferometer Space Antenna require metering structures of exceptional geometric stability in order to meet their science goals. Thermal expansion and contraction of these structures is typically a primary concern. The application of a known high-stability bonding method, hydroxide catalysis bonding, to a new structural material, ALLVAR Alloy 30, with the uniquely useful property among metals of a negative coefficient of thermal expansion is studied. We report on measurements of the shear breaking strength of Allvar mated with fused silica (glass), grade 5 Ti-6Al-4V (Ti64), and aluminum 6061-T6 (aluminum). Measured shear breaking strengths ranged from 3 to 16 MPa with a mean of ∼7.5 MPa. Initial series of tests indicated no significant correlation between bonding strength and surface roughness over the range of surface roughness tested. [DOI: 10.1117/1.JATIS.6.1.015007]

Keywords: hydroxide catalysis bonding; Allvar; LISA; LUVOIR; negative coefficient of thermal expansion; thermal stability.

Paper 19090 received Sep. 4, 2019; accepted for publication Jan. 30, 2020; published online Feb. 22, 2020.

1 Introduction

Many future space-based optical telescopes, such as Large UV/Optical/Infrared Surveyor (LUVOIR),[1] and gravitational wave observatories, such as Laser Interferometer Space Antenna (LISA),[2] rely on the dimensional stability of key structures over long periods of time. These structures are ideally made from materials with a very low effective coefficient of thermal expansion (CTE) such as ULE®, Zerodur®, or ClearCeram®. Unfortunately, these materials are rather brittle and difficult to machine. Integrating these materials into larger structures is also challenging and often requires additional mass to provide the necessary stiffness. The use of these materials in the load path during launch is very problematic due to potential for fracture. Furthermore, differential thermal expansion between the glass and the mounting structure can lead to deformations of the optical instruments.

Load-bearing structures in space missions often use titanium due to its superb strength to density ratio. One of the disadvantages of titanium is its CTE of nearly 10^{-5}/K, which is nearly 3 orders of magnitudes larger than the CTEs of ULE, Zerodur, and ClearCeram. Lately, a new material has become available. ALLVAR Alloy 30 (Allvar) has a negative CTE of −30 ppm/K at 25°C. Mating this alloy with a positive CTE metal such as titanium allows for the manufacturing of effectively zero CTE support structures, over specific length-scales and axes, with material properties similar to titanium.

We have a particular interest in Allvar mated to titanium as a potential structural material for LISA or LISA-like missions and, here, specifically as a spacer material within the telescopes (separating the primary from the secondary mirror), as a spacer material between the telescope and the optical bench, and as a mounting option for the telescope and the optical bench to

*Address all correspondence to Kaden J. Loring, E-mail: kloring@ufl.edu

the spacecraft. The primary and secondary mirror spacing application would require picometer $(\mathrm{pm})/\sqrt{\mathrm{Hz}}$ stability within LISA's measurement band centered around 1 mHz; demonstration of which is the goal of a currently ongoing series of experiments.

Here, we report on the study of a specific bonding technique—hydroxide catalysis bonding (HCB)—between Allvar and fused silica (glass), grade 5 Ti-6Al-4V (Ti64), and aluminum 6061-T6 (aluminum). Hydroxide bonds between other materials are known to be very thin, exhibit pm-stability, and have shown shear strength of several MPa in earlier tests. These bonds allow fairly strong structures to be built but not necessarily large load-bearing structures.

The immediate motivation of this study was to measure characteristic breaking strengths of Allvar mated to other common telescope materials by HCB. Provided the bonds are strong enough, as we found they are, the next step toward demonstration of zero-CTE spacers is to build an optical cavity with HCB in order to measure the dimensional stability of an Allvar–titanium composite at a sub-pm level. Building the cavity with HCB provides a desirable level of control in this initial stability measurement that a more practical mechanical bond may not since HCB has been proven to be pm-stable before.

1.1 *Hydroxide Catalysis Bonding*

HCB is a precision bonding method that has shown superior strength and thermal stability; this process was developed by Gwo[3] for the NASA Gravity Probe B mission.[4,5] HCB is best suited for silica-based materials and is conventionally used to bond silica, fused silica, ULE glass, and granite.[6] However, it is possible to make bonds between nonsilica-based materials with proper surface preparation and a bonding solution containing silicate ions.[7,8] The three major steps of HCB are (1) hydration and etching, (2) polymerization, and (3) dehydration, as described in Refs. 7 and 9.

The overarching requirement for the success of HCB is that a silicate-like network forms between the bonding surfaces. Gwo defines a silicate-like network as a "chemical-bond network with a structure similar to, but less rigid than bulk silicon dioxide."[3] A silicate-like network is "looser" than a bulk silicon dioxide network because more Si-OH (silanol) and Si-OM (cation terminating) groups are embedded and/or exposed rather than continuing the polymer structure.[5]

In the case of metal–glass or metal–metal HCB, as long as the alloy surface is oxidizable, the silicate ions may penetrate into pits and gain anchorage by the oxygen atoms along the surface to form the silicate-like network. The anchoring is provided via electrostatic forces, hydrogen bonds, and/or van der Waals bonds. This network is comprised of siloxane chains, which are formed in what Gwo calls the "hydroxide-catalyzed hydration/dehydration" process.[5]

Additional benefits of HCB include tunable settling time via solution pH, resistance to thermal shock, low bond thickness, and space-tested success in several previous (nonload bearing) applications, including LISA Path Finder.[4] Furthermore, the hydroxide solution turns into an optically transparent glassy layer, which in this case (see Fig. 1) allows one to see the metal

Fig. 1 Allvar–glass HCB bond, which exhibits visible transparency.

surface. It can also be made between relatively rough surfaces[4,6,7] as compared to optical contacting, which has stringent surface requirements. For instance, optical contacting usually requires a flatness of $\leq\lambda/10$,[7] whereas HCB with a sodium silicate solution is known to work with rougher surfaces[4] (also see results presented here).

Demonstrating HCB as a valid bonding technique for Allvar not only paves the way for $\mathrm{pm}/\sqrt{\mathrm{Hz}}$ stability tests of an Allvar–titanium structure itself but may also inform design concepts with optics bonded directly to Allvar–titanium metering structures. Furthermore, very few metal–metal HCB results have been published at the time of writing. Metal–metal HCB bonds may be of interest in the construction of low-CTE metering structures containing Allvar as the negative CTE material.

1.2 *Effect of Surface Roughness*

Much of the existing literature on HCB focuses on surface flatness.[4,10] The general consensus from this body of knowledge is that flatter surfaces result in stronger bonds. However, there are mixed statements regarding the effect of surface roughness on bond strength. Elliffe et al.[4] reported slightly greater breaking strengths for glass–glass bonds when a fine polish was used in lieu of a rough polish. Whereas, Preston[7] reports a negligible difference between rough and fine polished BK7–BK7 glass bonds. Furthermore, van Veggel et al.[6] states that "surface roughness is inconsequential for HCB." We performed a series of initial tests to (a) verify that Allvar can be bonded to glass and other metals using HCB and (b) establish a requirement for the needed surface roughness of the materials. The goal was to allow the construction of a "zero-CTE optical cavity" for currently ongoing dimensional stability tests at the pm level.

1.3 *Silica versus Nonsilica-Based Bonds*

HCB for nonsilica-based materials requires the addition of silicate ions in the bonding solution. Whereas, for a silica material in contact with a hydroxide solution, ample silicate ions may be liberated. Therefore, nonsilica-based bonds may be limited in strength by the concentration of silicate ions in the bonding solution. We anticipated that a bond involving two nonsilica materials should be weaker than one containing at least one silica material.

1.4 *Effect of Surface Oxidation*

In the case of nonsilica materials, the bond occurs within the surface oxide layer.[11] We expected that bonding to materials that support a thicker oxide layer would exhibit a greater breaking strength. While aluminum supports a 4-nm-thick oxide layer,[12] the oxide layer on Ti64 can be 10 nm or thicker.[13] Allvar is a Ti-based alloy and we expect it to have an oxide layer similar to Ti64. Therefore, Allvar–Ti64 bonds should exhibit higher breaking strengths than Allvar–aluminum bonds.

2 Methods

2.1 *Polishing*

Prior to bonding, all metal samples had to be polished to a desired level. On the other hand, glass samples were prepared by the manufacturer to $\lambda/10$ flatness and 40/20 scratch–dig finish. After receiving the cut metal flats and cylinders of Allvar, Ti64, and aluminum, each was initially surface-milled.

To test the effect of surface roughness on bond strength, a polishing procedure followed the surface-milling. At each level of polish, ranging from the roughest level of simple surface-milling to the finest level of 50-nm colloidal silica (CS), an allotment could be made of samples to be tested. Our primary levels of testing were "rough surfaces," which included surface-milled and 180 grit polished samples, and "fine surfaces," which included CS polished samples.

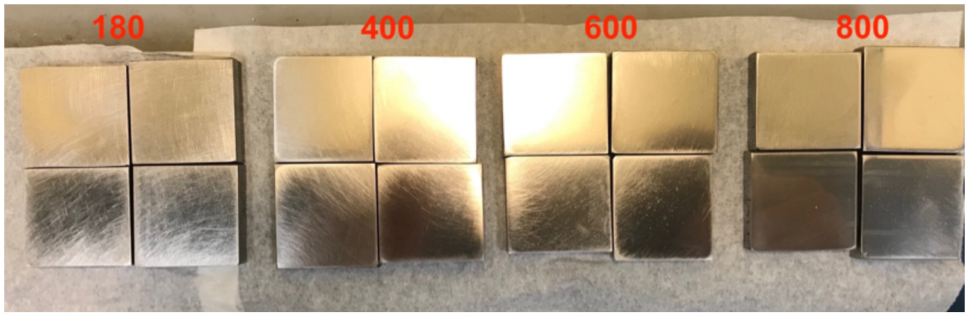

(a)

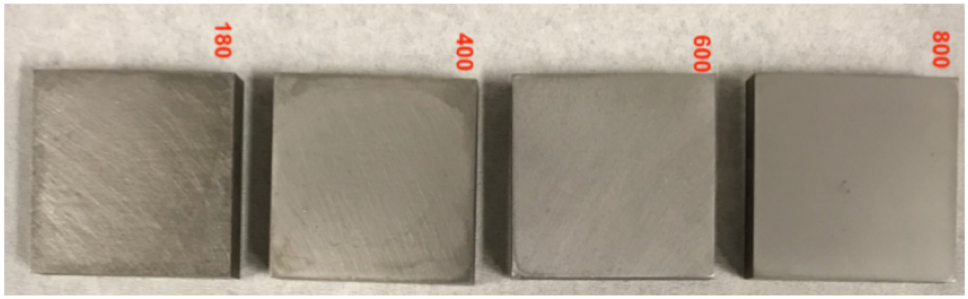

(b)

Fig. 2 Photographs showing the typical material surface at different stages of the polishing procedure of (a) Ti64 and (b) Allvar with different grits of abrasive paper. The abrasive grit of each step is noted in each image.

The first level of polish beyond surface-milling was 180 grit, which was performed for 1 min/bonding surface. Next followed 400, 600, and 800 grit polishing with silicon-carbide abrasives for 1 to 3 min each. Up to this point in the polish progression, none of the three types of metal should exhibit a mirror finish. Ti64 and aluminum samples at this point are "shiny" and exhibit some reflectivity, whereas Allvar samples are matte gray, but appear visibly smooth. Figure 2 shows the Ti64 and Allvar samples as they are polished to each level. The next polishing level used a 1-μm diamond suspension (DS) on a high-napped Metallographic ATLANTIS polishing pad for 3 to 5 min.

Finally, a 50-nm CS suspension was used on a Metallographic Black CHEM 2 porometric polymer pad. This final stage of polishing with CS is recommended to take 5 to 30 min for Allvar in order to achieve a mirror finish. For consistency, we restricted the time for all CS polished samples to 15 min. A visual comparison between DS and CS polished Allvar is shown in Fig. 3.

One witness Allvar sample for machine surface-milled, 180 grit, and CS polishes was imaged by a Bruker optical profilometer in order to quantify the roughness and flatness of the bonding

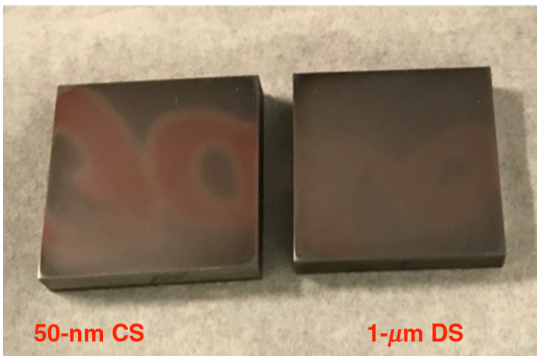

Fig. 3 Photograph showing the final surface finish of Allvar samples after the CS and DS polishing stages. The sample on the left (CS) is visibly less rough and exhibits significant specular reflection.

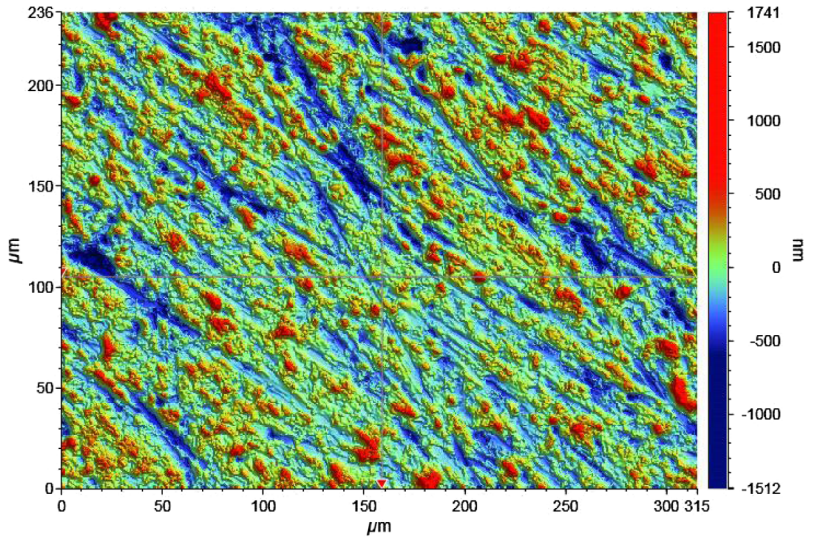

Fig. 4 Plot of surface roughness for a machine surface-milled Allvar sample.

surfaces. For the average surface roughness (Sa) measurement, five random scans of 0.3 mm × 0.3 mm were made on each sample at 20× magnification and with no applied filter. The five Sa measurements for each sample were then averaged for a more general estimation of roughness for each polish type. As expected, the value of Sa for 180 grit was much more than CS (1034 and 281 nm, respectively). The Sa measured for the machine surface-milled sample was only 200 nm. Note that the calculation for Sa can be misleading when the surface topographies are markedly different.[14] For example, the machine surface-milled sample exhibits long-uniform digs, whereas the manually applied 180 grit and CS polishes exhibit relatively large peaks and valleys but few extended digs (see Figs. 4–6).

The flatness was quantified in terms of maximum peak-to-valley deviation (Δz) and average waviness (Wa). The Δz measurement was averaged over the same five scans as described for Sa. The average value of Δz for each polish was on the order of 10 μm. Average waviness was measured over a scan area of 10 mm × 10 mm at 2.5× magnification. A Gaussian regression filter with a long wavelength pass of 80 μm was applied. The value of Wa for each of the three samples was ~200 nm. Average waviness is a measure of medium-scale surface features within the passband of the applied filter. Flatness specifications in the optics industry are typically

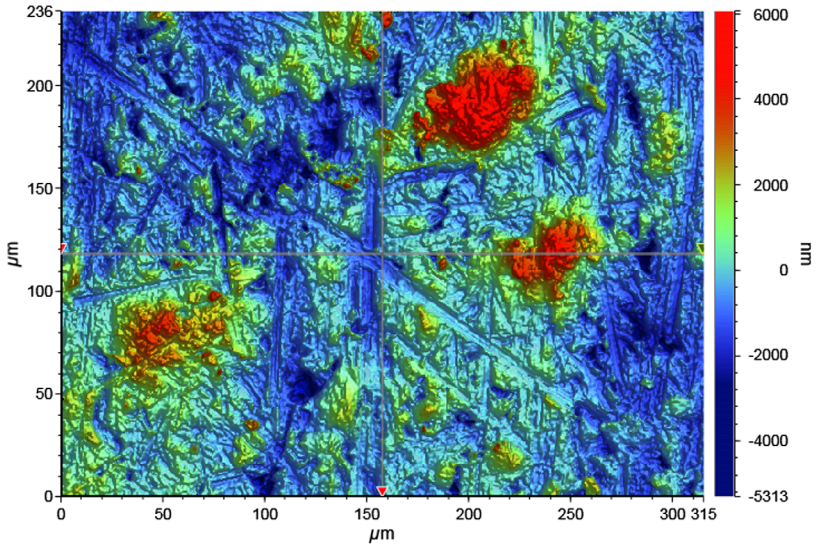

Fig. 5 Plot of surface roughness for a 180 grit polished Allvar sample.

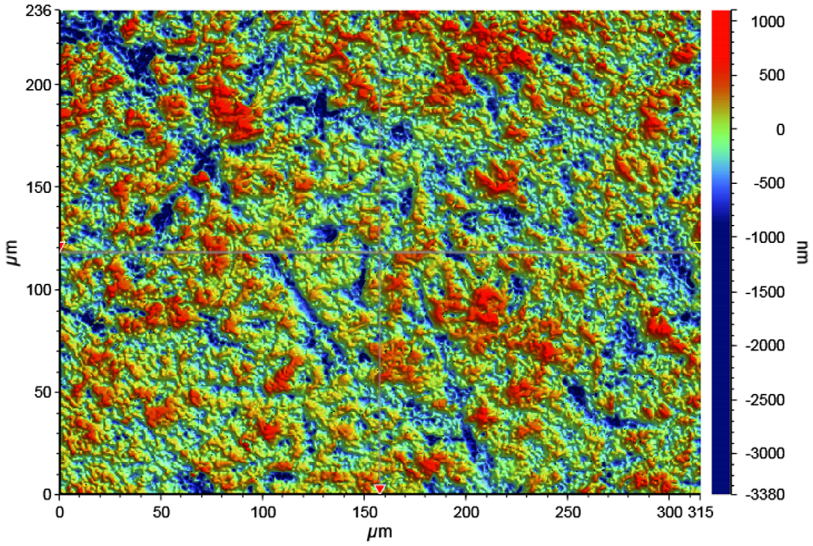

Fig. 6 Plot of surface roughness for a CS polished Allvar sample.

calculated from peak-to-valley deviation (Δz). From the measurements, a difference in flatness between the three polish types is not evident.

2.2 *Cleaning*

It is important that the bonding surfaces be free from any debris or foreign material for a proper bond to occur. The cleaning procedure we employed was inspired by Ref. 7. Samples were first washed with DI water to remove large particulates. Then a Kimtech wipe, wetted with methanol, was used to wipe the bonding surfaces. The samples were then placed, bond side up, in an isopropanol filled beaker within an ultrasonic bath for 15 min. Following the ultrasonic bath, the samples were removed from the beaker and wiped for a final time with another methanol wetted Kimtech wipe until all streaks and particulates were absent.

For the glass optics, the cleaning procedure was much shorter. Like the metal pieces, they were first washed in DI water to remove large particulates. Then, the optics were wiped with a methanol Kimtech wipe as a final cleaning to remove residual streaks and particulates.

The cleaning method chosen for this work is not the only one represented in literature. For instance, manual abrasion with cerium oxide and sodium bicarbonate paste is common.[6,15,16] This process is done to make the surfaces more hydrophilic, which further strengthens the bonds.[16] The Advanced Laser Interferometer Gravitational-wave Observatory (aLIGO) uses cerium oxide and sodium bicarbonate for HCB.[17] Additionally, cleaning bond surfaces inside UV ozone chambers is another common technique.[18,19] This is often the preferred method when the substrates to be bonded are too fragile for manual abrasion. Detailed studies of the impact of various cleaning methods on the bonding strength is beyond the purpose of our initial studies.

2.3 *Bonding*

In general, the solution chosen for HCB must be alkaline. Sodium hydroxide (NaOH) and potassium hydroxide (KOH) are standards for bonds made between silica-based materials. For nonsilica–based bonds, a sodium silicate solution is required.[7] The specific product used in our experiment was Millipore Sigma 338443, a solution of ~26.5% silicon dioxide (SiO_2) and ~10.6% sodium oxide (Na_2O). The chemical formula for the sodium silicate solution is given below:

$$(NaOH)_x(Na_2SiO_3)_y(H_2O)_z.$$

Much of HCB literature recommends 0.40 μL of bonding solution per cm^2 of bond area.[4,7,10] The cylindrical optics used in our experiment had a base area of 1.267 ± 0.001 cm^2; therefore,

each bond was allocated 0.51 μL of solution. The Sigma Millipore sodium silicate was diluted to a 1:4 sodium silicate to DI water solution. Preston's results indicated this ratio as his most successful concentration.[7] A micropipette was then used to position the solution. The cylinder was then carefully placed atop the solution deposit in order to minimize solution expelled beyond the bond area. A mass of a few grams is recommended to be placed atop the bond to ensure all surface irregularities are entirely filled. At this time, the samples were left to cure.

During preliminary testing, it was found that a 24-h curing period was likely insufficient; two bonds cured for 24 h exhibited a much lower breaking strength than two bonds cured for 48 h. As such, for the remainder of the first round of measurements, samples were allowed to cure for 48 h.

2.4 *Compression Shear Device*

The University of Florida (UF) developed a simple compression shear device (CSD) to apply a shear stress atop the bonding edge of a flat, parallel to the bond interface; it is described in Refs. 7 and 8. This stress mode is easily measured and allows us to compare our measurements with relevant previous research. Preston et al.[8] determined this as the "mode of failure with the least applied force," using similarly shaped samples.

The apparatus includes a strain-gauge type load cell manufactured by Transducer Techniques (model MLP-300.) The load cell has a rated capacity of 300 lbs. The load cell is attached to a DC-powered linear actuator, which moves the load cell and its pointed load cap into the sample to apply a breaking force.

A simple formula for stress applied to the bond area was developed so that output in mV from the load cell could be translated into MPa (see Eq. 1)

$$\sigma\,(\mathrm{Pa}) = \frac{X\,(\mathrm{mV})}{\gamma\,(\mathrm{mV/N}) \times A_b\,(\mathrm{m}^2)}. \tag{1}$$

The stress recorded (σ) is equal to the signal voltage X (in mV) divided by the mV/N calibration factor (γ) and bond area (A_b) over which the CSD is designed to isolate the force upon.

To provide quantitative results for breaking strength, it was necessary to calibrate the machine and find γ. Calibration was performed by placing 25 various known weights atop the load cell by means of a platform. The weights were measured with a calibrated digital scale and ranged from 33 through 214 lbs.

To match measurement conditions, the voltage was amplified by a factor of 100, filtered using a low-pass filter with a cutoff frequency of 3 kHz, and then recorded. Linear regression analysis of our calibration data produced $\gamma = 1.65$ mV/N, $R^2 = 0.994$ and a sample standard error of 8.19 mV. This results in a sample standard error for measured force of 4.96 N. This is insignificant in comparison to the weight used in calibration, which ranged from 140 to 950 N, as well as the average measured breaking force of 921.5 N.

2.5 *Compression Shear Test*

Once samples had cured for 48 h, they were placed into the CSD by inserting the cylindrical ends into the mobile loading platform (LP), as shown in Fig. 7. The LP has cavities that provide a firm hold on the sample. Screws and table clamps were used to fasten the LP in place so that it would not move during testing. The adjustable intermediary sledge was carefully positioned atop the edge of the metal flat such that shear stress was maximized while the torque moment was minimized.

An oscilloscope was programmed to record a small interval of time about a voltage spike trigger. This setup was designed to capture the signal evolution during fracturing such that a well-defined climb, peak, and then drop would be recorded. In most samples, a nearly complete and instantaneous fracture occurred such that there was only a single voltage peak. In glass–glass tests, there were often multiple peaks; each peak representing a partial fracture within the LP cavity. It was always the first peak that defined our breaking strength measurement of the bond.

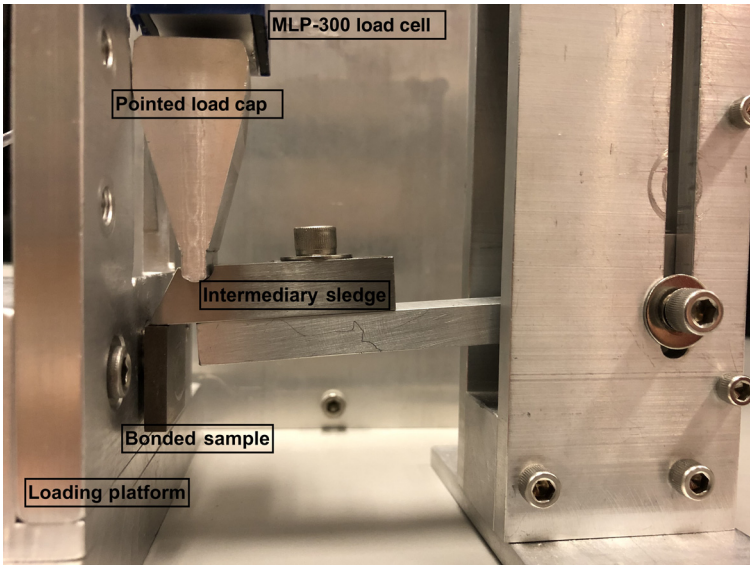

Fig. 7 Labeled photograph with constituent parts of the CSD used to measure the shear breaking strength for the tested bonds.

Fracture characteristics can vary widely. In the case of metal–glass bonds, the bonded sample may fracture completely through the bond interface, completely within the homogeneous glass, or as a partial homogeneous fracture. In the latter two, the metal piece retains a significant amount of the glass meaning the failure did not occur completely at the bond interface. For reference, two types of fractures are shown in Figs. 8 and 9.

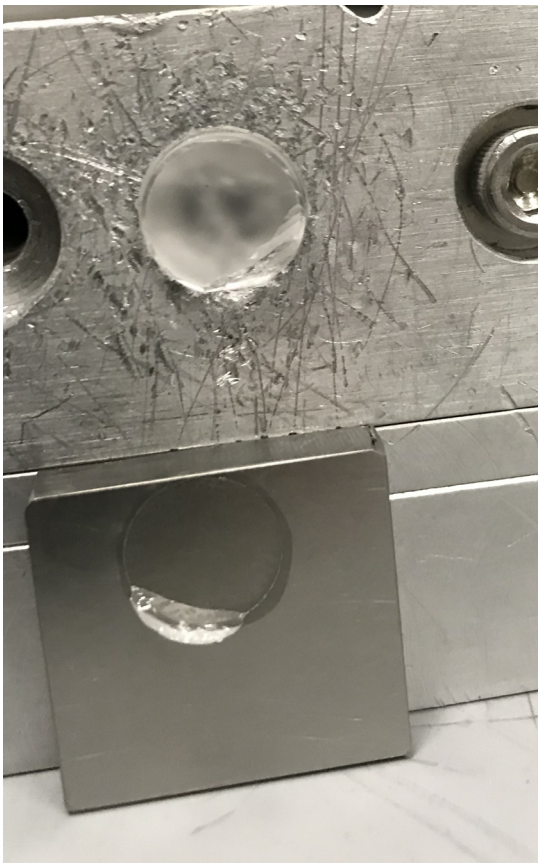

Fig. 8 Photograph of a partial homogeneous fracture in an Allvar–glass bond.

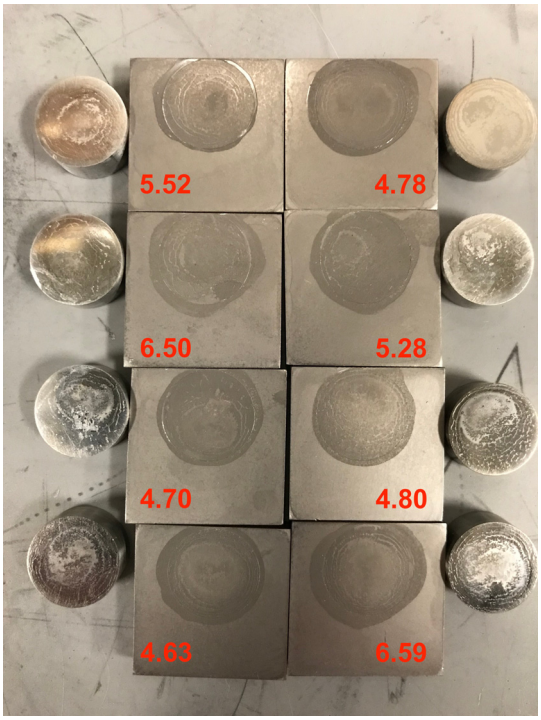

Fig. 9 Photograph of homogeneous metal–metal bond fractures with measured bond shear strength in MPa shown in red.

As an example of the measurement process, Fig. 10 shows the time series of four 180 grit Allvar–aluminum compression shear tests (CST) with the amplified load cell signal plotted on the y axis. The small perturbation in the signal at ~ -0.05 s relative to the trigger is due to contact noise between the load cap and intermediary sledge. Of this small example group, the peak signal was measured for sample 65 (S65) at ~2.43 V. This corresponds to a shear breaking strength of ~11.6 MPa.

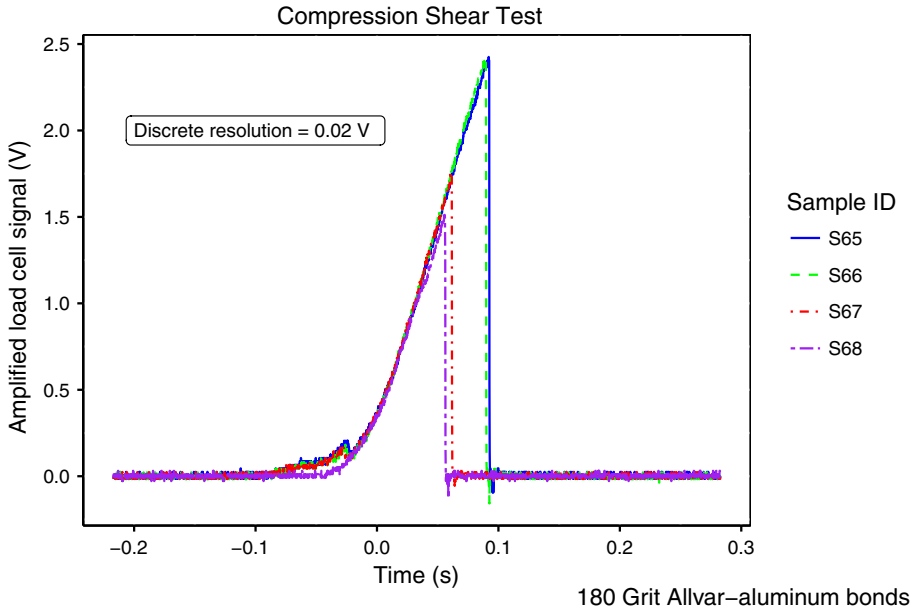

Fig. 10 Example time series of amplified and filtered load cell outputs during the shearing of four Allvar–aluminum bonds with 180 grit surface finish.

The discrete resolution of the oscilloscope used during the experiment was 20 mV, well above the calibration standard deviation of 8 mV. For most of the breaking strengths we measured, the 20-mV resolution made up <1% of the output voltage.

3 Results

3.1 *Metal–Glass Breaking Strengths*

Figure 11 summarizes the bond shear measurements of the metal–glass bonds. To compare the effect of a rough or fine surface polish, 21 Allvar–glass bonds made with either surface-milled or 180 grit surface polishes and 21 of the same bonds made with 50-nm CS polish were tested. The milled and 180 grit samples are grouped into the same "rough" polish category, as both visual inspection and indistinguishable breaking strengths between these two such polish levels led us to classify each equivalently. In addition, a smaller group of nine Ti64–glass bonds at 180 grit were tested for comparison.

The sample standard deviation is included with each group as a representation of the experimental error (see Fig. 11). The data points have been horizontally spaced in each of the following plots, which contain point markers to avoid overplotting. A solid line across a given boxplot denotes the median and a dashed line denotes the mean. The cumulative mean for all data points within a plot is stated at the bottom right of the following two boxplot figures (Figs. 11 and 12) for reference.

3.2 *Metal–Metal Breaking Strengths*

The same surface polish test as metal–glass bonds was compared in metal–metal bonds. In this case, however, both bond types, Allvar–Ti64 and Allvar–aluminum, were tested at 180 grit and CS. No surface-milled samples were used for this data group (see Fig. 12).

3.3 *Complete CST Summary*

In total, 152 CSTs were performed on various sample types. Data for only the aforementioned bond types are summarized in Figs. 13 and 14, which are grouped by bond type.

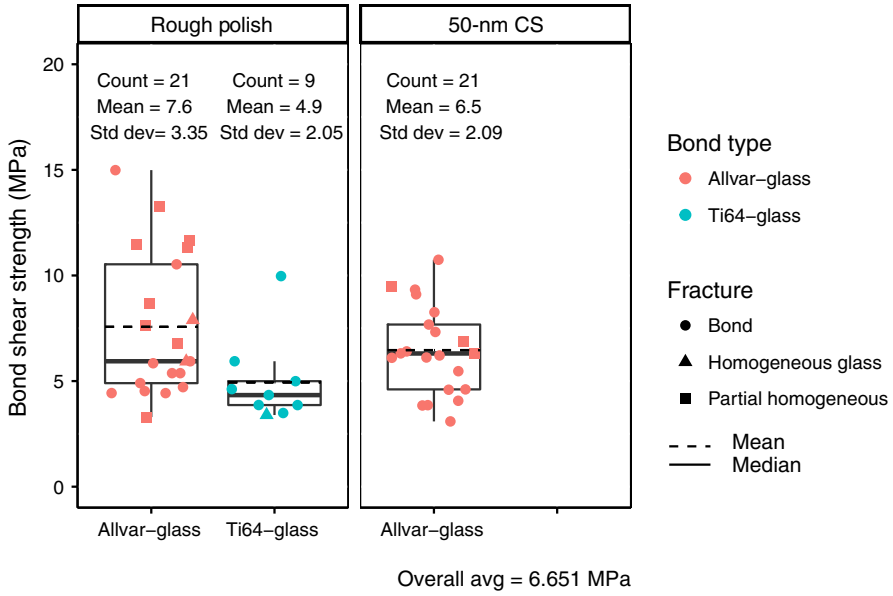

Fig. 11 Box plots showing the distribution of measured bond shear strengths of the Ti64–glass and Allvar–glass bonds, for two different levels of surface finish. The box height denotes interquartile range. The point markers are spaced horizontally to avoid overplotting.

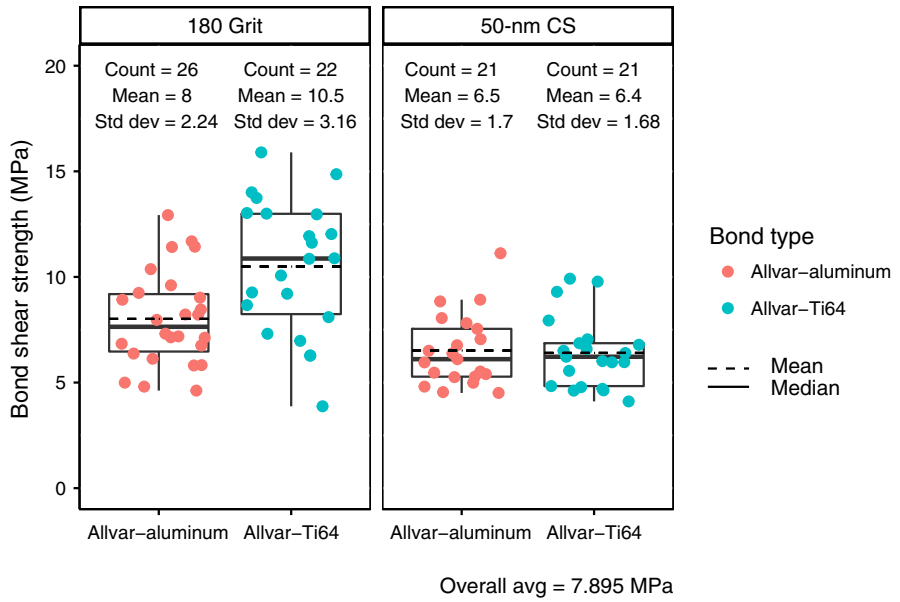

Fig. 12 Box plots showing the distribution of measured bond shear strengths of the Allvar–aluminum and Allvar–Ti64 bonds, for two different levels of surface finish. The box height denotes interquartile range. The point markers are spaced horizontally to avoid overplotting.

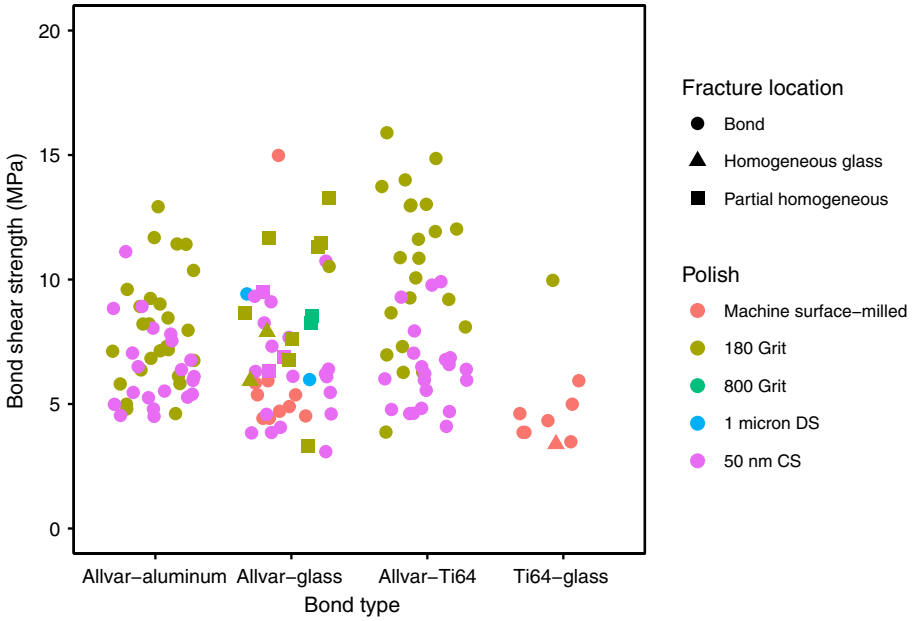

Fig. 13 Summary of measured bond shear strengths for Allvar–glass, Ti64–glass, Allvar–aluminum, and Allvar–Ti64 bond types and tested surface finishes. The point markers are spaced horizontally to avoid overplotting.

4 Discussion

4.1 *Allvar-Hydroxide Catalysis Bonding*

The primary objective of our experiment was to prove the application and determine the shear breaking strength of HCB in Allvar–glass, Allvar–Ti64, and Allvar–aluminum bonds to explore if it is suitable for our planned optical cavity experiments. The measured breaking strengths also entice further exploration of HCB bonded Allvar–titanium and Allvar–glass structures for

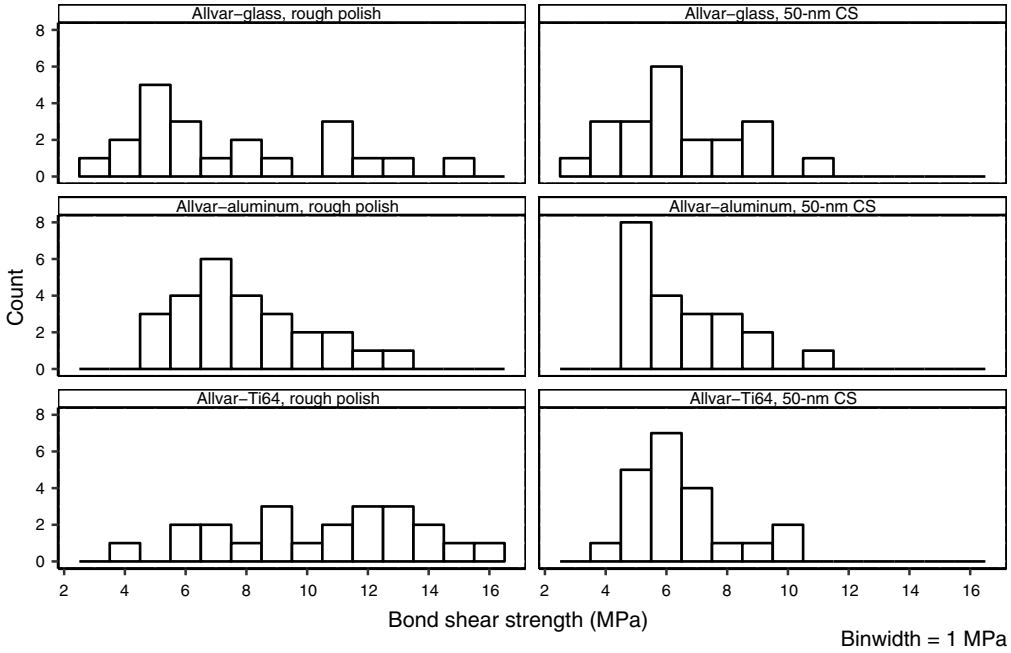

Fig. 14 Histograms of measured bond shear strengths for Allvar–glass, Allvar–aluminum, and Allvar–Ti64 bond types and tested surface finishes. The binwidth for each histogram is 1 MPa. Rough polish includes both surface-milled and 180 grit polishes.

potential use in a broad range of nonload-bearing applications, including optical telescopes and interferometric gravitational wave observatories. For all three bond types, regardless of the polish, mean bond shear strengths on the order of several MPa were observed as shown in Figs. 11 and 12.

While other experiments[4,7] have shown similar results for HCB shear breaking strengths, this is the first time Allvar has been used as one of the bonded materials. Furthermore, as described in Ref. 10, the relatively large variability in breaking strengths is not uncommon for HCB. As Allvar has now been shown to be a successful candidate for HCB, further experiments with more realistic Allvar-composite structures could be tested in other modes of stress, such as vibrational testing and thermal cycling under various loads.

4.2 *Surface Roughness and Breaking Strength*

Surface-milled and 180 grit polishes as a "rough" control and the 50-nm CS polished samples as a "fine" polish comparison were used to study the breaking strength as a function of surface roughness. While mean breaking strengths for rough polish groups are slightly higher than their fine polish counterpart, no conclusion can be drawn over the range of polishes tested due to relatively large experimental variation.

For instance, the average percent variance from the mean over the seven breaking strengths shown in Figs. 11 and 12 is nearly 25%, indicating that most of the spread in our data is from physical variations in the breaking strength of the bonds and not measurement uncertainty. This nonuniformity may be associated with uncontrolled variations in the polishing, cleaning, bonding, or CST procedures. As an example, over the course of many polishing cycles, the metal flats and cylinders may have developed rounded edges and surface mismatch, as Preston speculated.[7]

Despite the large variations, it might be of interest that the spread in bond shear strengths is greater for all the rough polish samples. This can be seen from the greater standard deviation for rough as opposed to fine polishes for corresponding bond types. For example, while the 180 grit Allvar–Ti64 bonds had a mean bond shear strength of 10.5 MPa compared to 6.4 MPa for CS, the standard deviation was 3.16 and 1.68 MPa, respectively (see Fig. 12). Furthermore, Fig. 14 visually depicts the larger spread but greater maxima in shear strength for rough polishes. These results could imply a trade-off between maximal bond shear strength and consistency.

It should be noted when comparing Allvar–glass bonds, the fracture location observed in the fine polish set was more consistently a "pure bond" fracture. The rough polish set had 10 partial or complete homogeneous fractures out of the 21 tests, whereas the fine polish set only had 3 out of 21. We speculate that a fracture at least partially within the homogeneous glass indicates a stronger bond as the bulk glass broke in lieu of the bond material.

Qualitatively, we observed in the case of both metal–glass and metal–metal samples, the texture along the bond area postfracture of a rough polish may be described as having coarse, glass-like particulates that cling to the metal surface strongly. For fine polish samples, the residual bond material is more sand-like, easily removed from the metal surface with manual abrasion, and of smaller particle size than that present on the rough polish samples. It seems reasonable to assume that stronger siloxane anchors are made with a rough polish surface based on these qualitative observations. At a microscopic level, the rough polished surfaces are more rugged, which could lend itself to this anchoring phenomenon.

4.3 *Nonsilica-Based Bonds*

We expected, prior to this experiment, that metal–glass bonds would exhibit stronger breaking strengths than metal–metal bonds. The rationale was twofold: 1) nonsilica-based materials require silicate ions in the HCB solution and 2) siloxane-chain anchoring occurs within the oxidation layer present at the surface of the nonsilica material, rather than within bulk silica. The overall average breaking strength for the four types of metal–metal bonds (see Fig. 12) compared with the three types of metal–glass bonds (see Fig. 11) is greater by more than 1 MPa. A *t*-test and Mann–Whitney–Wilcoxon test reveal little statistical significance to this difference in mean bond shear strengths, and there are also some experimental concerns in comparing these values. In comparing metal–glass results to metal–metal results, it should be noted that many metal–glass fractures occurred within the homogeneous glass or as a partial homogeneous fracture within the LP holder. Whereas, metal–metal bonds obviously fractured at the bond site. This might suggest that in some cases we are measuring the breaking strength of pure glass in some undesired mode of stress rather than the bond shear strength itself for metal–glass bonds. Practically however, the metal–metal bonds have exhibited shear strength well within one standard deviation, if not on par, to that of metal–glass bonds (see Figs. 11 and 12).

Further analysis and/or revision of the dynamics of the CSD should be performed to ensure only a pure shear stress at the bond is applied to the samples and that the fractures occur at the bond site for all future samples tested.

4.4 *Surface Oxidation*

As nonsilica-based materials bond with HCB via surface oxidation, we tested whether Allvar would form a stronger bond with Ti64 than with aluminum due to Ti64's thicker oxide layer. This follows from results in Refs. 7 and 15. In the former, metal–metal bonds involving oxidation resistant materials failed. While in the latter, silica–silica bonds showed diminishing breaking strengths with thinner oxidation layers.

Our measurements do not provide any quantitative confirmation of this assumption (see Fig 12). While the average breaking strength for Allvar–Ti64 bonds was 17% higher compared to Allvar–aluminum bonds, the difference is only visible in 180 grit (rough) polished surfaces and not in the 50-nm CS (fine) polished surfaces. This is (a) not sufficiently statistically relevant and (b) more likely an artifact associated with the real surface roughness, which does not only depend on the polishing method but also on the material itself; titanium is much harder than aluminum. Further work in this direction is needed.

5 Conclusion

We have successfully demonstrated HCB for Allvar–glass, Allvar–Ti64, and Allvar–aluminum bonds. These bonds exhibit very similar shear breaking strengths and behavior to other metal–glass and metal–metal bonds. Further, the contribution of surface roughness to shear breaking

strength in the aforementioned bond types was explored. Measurements from this comparison indicate a higher breaking strength when using rough (180 grit and surface-milled samples) as opposed to fine (50-nm CS) polished surfaces. A smaller variance in breaking strengths was measured for the fine polished samples, possibly meaning a greater consistency in bonding. However, a relatively large variance in all measurements means that no firm conclusions can be made on the two latter relationships at this time.

To develop a flight qualifiable process for space missions, such as LISA or LUVOIR, further study is needed to better understand variables affecting bond shear strength and to lower the standard deviation of bond strength measurements. However, our results should open the door to explore implementations of ALLVAR Alloy 30 with HCB in applications where near-zero CTE, high thermal conductivity, reasonable bond strength, and vacuum compatibility are all design requirements.

Future work includes the construction of an Allvar–titanium-based optical cavity using HCB to bond the metals and the mirrors together. The CTE of the structure as well as the intrinsic dimensional stability at the pm level will then be measured to look for effects beyond thermal expansion, such as material creep.

Assuming that this simple composite can reach a dimensional stability similar to Zerodur and ULE in similar thermal environments, HCB bonds could be used for non- or low-load-bearing assemblies in fairly simple thermomechanical geometries. For higher load-bearing assemblies, other techniques, such as welding or bolting, have to be evaluated to also take advantage of the superior strength of Allvar and titanium. However, the impact of the heat required for welding or of the more complicated thermomechanical geometry will add complexity to the design process. These studies are, however, beyond the scope of this paper but currently under way at UF.

Acknowledgments

This work was funded by NASA SBIR 80NSSC18P2061. We also like to thank Dr. Jeffrey Livas (GSFC) for very useful discussions and comments.

References

1. M. R. Bolcar et al., "Initial technology assessment for the Large-Aperture UV-Optical-Infrared (LUVOIR) mission concept study," *Proc. SPIE* **9904**, 99040J (2016).
2. P. Amaro-Seoane et al., "Laser interferometer space antenna," A proposal in response to the ESA call for L3 mission concepts, https://www.elisascience.org/files/publications/LISA_L3_20170120.pdf (2017).
3. D. Gwo, "Hydroxide-catalyzed bonding," U.S. Patent No. US6548176B1 (2003).
4. E. J. Elliffe et al., "Hydroxide-catalysis bonding for stable optical systems for space," *Classical Quantum Gravity* **22**, S257–S267 (2005).
5. D.-H. Gwo, "Ultraprecision bonding for cryogenic fused-silica optics," *Proc. SPIE* **3435**, 136–142 (1998).
6. A. van Veggel et al., "Hydroxide catalysis bonding of silicon carbide," *J. Eur. Ceram. Soc.* **28**(1), 303–310 (2008).
7. A. Preston, "Stability of materials for use in space-based interferometric missions," PhD Thesis, University of Florida (2010).
8. P. Preston, B. Balaban, and G. Mueller, "Hydroxide bonding strength measurements for space-based optical missions," *Int. J. Appl. Ceram. Technol.* **5**(4), 365–372 (2008).
9. A. A. van Veggel et al., "Strength testing and SEM imaging of hydroxide-catalysis bonds between silicon," *Classical Quantum Gravity* **26**, 175007 (2009).
10. A.-M. A. van Veggel and C. J. Killow, "Hydroxide catalysis bonding for astronomical instruments," *Adv. Opt. Technol.* **3**, 293–307 (2014).
11. H. S. Kim and T. L. Schmitz, "Shear strength evaluation of hydroxide catalysis bonds for glass–glass and glass–aluminum assemblies," *Precis. Eng.* **37**(1), 23–32 (2013).
12. B. C. Bunker et al., "Hydration of passive oxide films on aluminum," *J. Phys. Chem. B* **106**(18), 4705–4713 (2002).

13. J. Pouilleau et al., "Structure and composition of passive titanium oxide films," *Mater. Sci. Eng.: B* **47**(3), 235–243 (1997).
14. "Michigan metrology surface texture parameters glossary," Sa and Sq, Provided by Bruker Nano Surfaces Division (2014).
15. N. L. Beveridge et al., "Low-temperature strength tests and SEM imaging of hydroxide catalysis bonds in silicon low-temperature strength tests and SEM imaging of hydroxide catalysis bonds in silicon," *Classical Quantum Gravity* **28**, 229501 (2011).
16. M. Phelps et al., "Strength of hydroxide catalysis bonds between sapphire, silicon, and fused silica as a function of time," *Phys. Rev. D* **98**, 122003 (2018).
17. H. Armandula and M. van Veggel, "Silicate bonding procedure (hydroxide-catalysis bonding)," LIGO Technical Note E050228 (2010).
18. L. Prokhorov et al., "Upper limits on the mechanical loss of silicate bonds in a silicon tuning fork oscillator," *Phys. Lett. A* **382**(33), 2186–2191 (2018).
19. R. Douglas, "Aspects of hydroxide catalysis bonding of sapphire and silicon for use in future gravitational wave detectors," PhD Thesis, University of Glasgow (2016).

Kaden J. Loring is an undergraduate in the Department of Physics, University of Florida (UF). He will graduate with a BS degree in physics in May 2020 and pursue a PhD thereafter. His research interests include optics, remote sensing, applied physics, plasma physics, and astrophysics. His prior research includes space system design, hybrid electric vehicle powertrain optimization, remote sensing, and atmospheric physics.

Luis F. Ortega is a graduate student in the Department of Physics, UF. He has worked on instrument science for interferometric gravitational-wave observatories (LIGO, Advanced LIGO, and LISA). His research interests include all aspects of laser interferometry for fundamental physics and astronomy projects.

James A. Monroe received his PhD from Texas A&M University. As a materials scientist at ALLVAR, he has been the principal investigator of several NSF and NASA SBIR awards. His technical expertise is in alloy processing, microstructure and mechanical property relationships, shape memory alloys, high-temperature and metamagnetic shape memory alloys, twinning and thermoelastic martensitic transformations, powder metallurgy, strain glasses, and ferroic glasses. His current research is focussed on the manufacturing of tailored and negative thermal expansion alloys for athermal optics applications.

Jeremy S. McAllister is an engineering manager at ALLVAR. He received his BS degree in industrial engineering from Mississippi State University and MS degree in engineering systems management from Texas A&M University. His work is focused on the manufacturing processes and quality control of innovative tailored and negative thermal expansion ALLVAR alloys.

Xavier Huerta received his BS and MS degrees in mechanical engineering from Texas A&M University in College Station. While at Texas A&M, his research included investigating and tailoring negative thermal expansion in shape memory alloys.

Guido Mueller is a professor in the Department of Physics, UF. He received his PhD from the University of Hannover. He has worked on interferometric gravitational-wave observatories (LIGO, Advanced LIGO, and LISA) and dark matter detectors (ALPS). His research interests include all aspects of laser interferometry for fundamental physics and astronomy projects.

Paul Fulda is an assistant professor of experimental astrophysics at UF. He received his PhD in physics from the University of Birmingham, where he studied precision interferometry for LIGO applications. He has since worked on laser interferometry for gravitational wave detection on ground (Advanced LIGO) and in space (LISA), and continues to actively research in both areas.